

DRAFT VERSION AUGUST 30, 2023

Typeset using L^AT_EX preprint style in AASTeX631

Constraining the binarity of black hole candidates: a proof-of-concept study of Gaia BH1 and Gaia BH2

TOSHINORI HAYASHI ^{1,2} YASUSHI SUTO ^{2,3} AND ALESSANDRO A. TRANI ^{4,3,5}

¹*Yukawa Institute for Theoretical Physics, Kyoto University, Kyoto 606-8267, Japan*

²*Department of Physics, The University of Tokyo, Tokyo 113-0033, Japan*

³*Research Center for the Early Universe, School of Science, The University of Tokyo, Tokyo 113-0033, Japan*

⁴*Niels Bohr Institute, University of Copenhagen, Blegdamsvej 172100 Copenhagen, Denmark*

⁵*Okinawa Institute of Science and Technology Graduate University, Okinawa 904-0495, Japan*

(Received 2023 July 1; Revised 2023 August 25; Accepted 2023 August 28)

Submitted to ApJ

ABSTRACT

Nearly a hundred of binary black holes (BBHs) have been discovered with gravitational-wave signals emitted at their merging events. Thus, it is quite natural to expect that significantly more abundant BBHs with wider separations remain undetected in the universe, or even in our Galaxy. We consider a possibility that star-BH binary candidates may indeed host an inner BBH, instead of a single BH. We present a detailed feasibility study of constraining the binarity of the currently available two targets, Gaia BH1 and Gaia BH2. Specifically, we examine three types of radial velocity (RV) modulations of a tertiary star in star-BBH triple systems; short-term RV modulations induced by the inner BBH, long-term RV modulations induced by the nodal precession, and long-term RV modulations induced by the von Zeipel-Kozai-Lidov oscillations. Direct three-body simulations combined with approximate analytic models reveal that Gaia BH1 system may exhibit observable signatures of the hidden inner BBH if it exists at all. The methodology that we examine here is quite generic, and is expected to be readily applicable to future star-BH binary candidates in a straightforward manner.

Keywords: techniques: radial velocities - celestial mechanics - (stars:) binaries (including multiple): close - stars: black holes

Corresponding author: Toshinori Hayashi
toshinori.hayashi@yukawa.kyoto-u.ac.jp

1. INTRODUCTION

Since the first discovery of GW150914 (Abbott et al. 2016), more than 90 candidates for binary black holes (BBHs) have been reported so far (The LIGO Scientific Collaboration et al. 2021). The formation and evolution of such BBHs are one of the important unsolved questions in astrophysics, and there are a variety of proposed scenarios; (1) final stage of isolated massive binary stars (e.g. Belczynski et al. 2002, 2007, 2012, 2016a,b; Dominik et al. 2012, 2013; Kinugawa et al. 2014, 2016; Spera et al. 2019), (2) dynamical capture in dense clusters (e.g. Portegies Zwart & McMillan 2000; O’Leary et al. 2009; Rodriguez et al. 2016; Tagawa et al. 2016; Fragione et al. 2020; Trani et al. 2022), (3) binary formation channel of primordial black holes (e.g. Ioka et al. 1999; Bird et al. 2016; Sasaki et al. 2016, 2018; Kocsis et al. 2018), and (4) evolution of wide binaries under the effect of galactic tide or cumulative flybys (e.g. Michaely & Perets 2016, 2019; Michaely & Naoz 2022). Regardless of those different formation scenarios, their progenitors are expected to have a longer orbital period. The subsequent dynamical evolution decreases their orbital energy and angular momentum, and eventually leads to the BBH merger events that are detectable using gravitational wave (GW) observations. Therefore, it is natural to expect that more abundant wide-separation BBHs remain undetected in the universe, or even in our Galaxy.

In order to search for BBHs with relatively long orbital periods that cannot be probed with GWs, Hayashi et al. (2020) and Hayashi & Suto (2020) pointed out that a BBH orbited by a tertiary star would be detectable in optical spectroscopic surveys from the radial velocity (RV) modulations of the tertiary star; the inner BBH produces the observable RV modulations of the star in short (a half of the orbital period of the BBH) and long (a nodal precession timescale and/or the von Zeipel-Kozai-Lidov timescale) terms. They examined the feasibility of the strategy from three-body simulations for hypothetical triple systems of an inner BBH and an outer tertiary star, and proposed that the methodology can distinguish between the single black hole (BH) and BBH when applied to the future star-BH binary candidates from on-going Gaia (Gaia Collaboration et al. 2016) and TESS (Ricker et al. 2014) surveys (e.g. Kawanaka et al. 2016; Breivik et al. 2017; Mashian & Loeb 2017; Yamaguchi et al. 2018; Masuda & Hotokezaka 2019; Shikauchi et al. 2020; Chawla et al. 2022).

Indeed, star-BH binary candidates, Gaia BH1 and Gaia BH2, recently discovered from Gaia DR3 astrometric data (Gaia Collaboration et al. 2022; El-Badry et al. 2023a,b; Chakrabarti et al. 2023; Tanikawa et al. 2023) would provide a good opportunity to directly check the methodology. Gaia BH1 is a binary of a $\sim 1M_{\odot}$ main sequence star and a $\sim 10M_{\odot}$ dark companion, with an orbital period $P_{\text{obs}} \sim 190$ days (El-Badry et al. 2023a; Chakrabarti et al. 2023; see also Rastello et al. 2023). Gaia BH2 was first discovered by Tanikawa et al. (2023) using Gaia astrometry, and later more robustly identified combining the follow-up RV observations by El-Badry et al. (2023b). Gaia BH2 is a binary of a $\sim 1M_{\odot}$ red giant and a $\sim 9M_{\odot}$ dark companion, with $P_{\text{obs}} \sim 1300$ days. The best-fit values of their system parameters are listed in Table 1.

Due to the limited precision and duration of the current spectroscopic monitoring observations, it is not possible to prove the presence of an inner BBH, instead of a single dark companion, in either system. Nevertheless, those systems are useful as a proof-of-concept in constraining the binarity of the dark companion for future star-BH binary candidates.

We first consider the short-term RV modulations on the timescale of half the inner orbital period. We next move on to the long-term RV modulations, which become important for inclined triples. We

Table 1. Best-fit parameters for Gaia BH1 and BH2 systems

system parameter	symbol	Gaia BH1	Gaia BH2
star mass	m_*	$0.93 \pm 0.05 M_\odot$	$1.07 \pm 0.19 M_\odot$
companion mass	m_c	$9.62 \pm 0.18 M_\odot$	$8.94 \pm 0.34 M_\odot$
eccentricity	e_{obs}	0.451 ± 0.005	0.5176 ± 0.0009
pericenter argument	ω_{obs}	$12.8 \pm 1.1 \text{ deg}$	$130.9 \pm 0.4 \text{ deg}$
longitude of ascending node	Ω_{obs}	$97.8 \pm 1.0 \text{ deg}$	$266.9 \pm 0.5 \text{ deg}$
RV semi-amplitude	K_{obs}	$66.7 \pm 0.6 \text{ kms}^{-1}$	$25.23 \pm 0.04 \text{ kms}^{-1}$
orbital inclination	I_{obs}	$126.6 \pm 0.4 \text{ deg}$	$34.87 \pm 0.34 \text{ deg}$
orbital period	P_{obs}	$185.59 \pm 0.05 \text{ days}$	$1276.7 \pm 0.6 \text{ days}$
semi-major axis	a_{obs}	$1.40 \pm 0.01 \text{ au}$	$4.96 \pm 0.08 \text{ au}$

 NOTE—The best-fit values are adopted from [El-Badry et al. \(2023a\)](#) for Gaia BH1 and [El-Badry et al. \(2023b\)](#) for Gaia BH2.

put constraints, as one application, on the binarity of dark companions in Gaia BH1 and Gaia BH2. For reference, Figure 1 shows the configuration of a triple that we consider in the present paper.

The rest of paper is organized as follows. Section 2 examines the short-term RV modulations. We first discuss the short-term semi-amplitude predicted from an analytic approximation for coplanar and circular triples. Then, we show that the outer eccentricity, such as those for Gaia BH1 and Gaia BH2, significantly increases the simple prediction by direct three-body simulations. Next, section 3, focuses on the long-term RV modulations induced by the nodal precession for moderately inclined triples. We also discuss analytic predictions first, and then examine their validity using three-body simulations. Section 4 considers more significantly inclined triples in which the von Zeipel-Kozai-Lidov (ZKL) oscillations ([von Zeipel 1910](#); [Kozai 1962](#); [Lidov 1962](#)) play an important role. Finally, we summarize the constraints on Gaia BH1 and Gaia BH2, and discuss a future prospect in section 5.

2. SHORT-TERM RV MODULATIONS

For a coplanar triple system, the inner binary efficiently induces short-term wobbles of the tertiary, with about a half the inner orbital period P_{in} . For inclined triples, however, the additional long-term RV modulations are generated due to the misalignment between the inner and outer orbital angular momenta. This section focuses on coplanar triples, and discusses the amplitude of the short-term RV modulations using an analytic approximation and numerical simulations. The long-term RV modulations for inclined triples will be discussed in later sections.

2.1. Analytic estimates

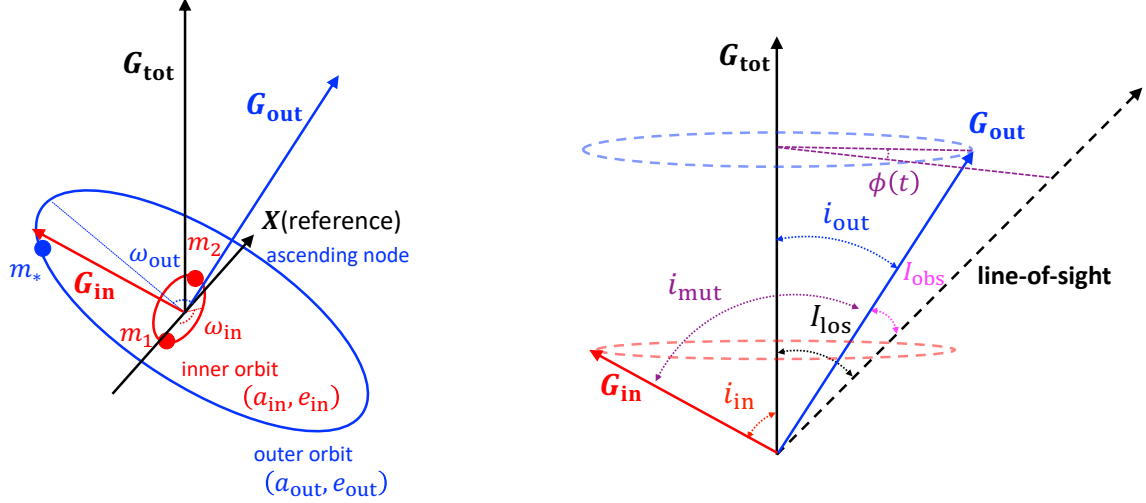


Figure 1. Schematic illustration of a triple system configuration that we consider in the present paper. The orbital angles are defined with respect to the reference Cartesian frame whose origin is set to be the barycenter of the inner orbit. The left panel shows the inner and outer orbits, and the right panel defines various angles specifying the orientations of the total (\mathbf{G}_{tot}), inner (\mathbf{G}_{in}) and outer orbital angular momenta of the system (\mathbf{G}_{out}); the mutual inclination between the inner and outer binaries (i_{mut}), the orbital inclinations of the inner (i_{in}) and outer (i_{out}) binaries with respect to \mathbf{G}_{tot} , the inclination of the line-of-sight with respect to \mathbf{G}_{tot} (I_{los}), and the inclination of the outer orbit with respect to the observer’s line-of-sight (I_{obs}). The time-dependent azimuthal angle of \mathbf{G}_{out} relative to the line-of-sight is $\phi(t)$.

The short-term RV modulations for coplanar and circular triples are, to the leading order of $a_{\text{in}}/a_{\text{out}}$, analytically approximated as (e.g. Hayashi et al. 2020)

$$\begin{aligned}
 V_{\text{short}}(t) = & -\frac{15}{16}K_{\text{short}} \cos[(2\nu_{\text{in}} - 3\nu_{\text{out}})t + 2\theta_{\text{in}} - 3\theta_{\text{out}}] \\
 & + \frac{3}{16}K_{\text{short}} \cos[(2\nu_{\text{in}} - \nu_{\text{out}})t + 2\theta_{\text{in}} - \theta_{\text{out}}],
 \end{aligned} \tag{1}$$

where ν_{in} , ν_{out} , θ_{in} and θ_{out} are the orbital frequencies and the true longitudes (the angle between a body’s location and the ascending node) for inner and outer orbits, respectively. The true longitudes θ_{in} and θ_{out} in equation (1) are expressed as

$$\theta_{\text{in}} \equiv f_{\text{in}} + \omega_{\text{in}} \tag{2}$$

and

$$\theta_{\text{out}} \equiv f_{\text{out}} + \omega_{\text{out}} \tag{3}$$

for eccentric orbits, where f_{in} , f_{out} , ω_{in} and ω_{out} are the true anomalies and the pericenter arguments of inner and outer orbits, respectively, evaluated at the initial epoch. Incidentally, we define ν_{in} and ν_{out} as orbital frequencies of inner and outer orbits throughout the present paper, which should not be confused with the true anomalies (denoted by f here).

In equation (1), K_{short} corresponds to a characteristic semi-amplitude of the short-term RV modulations defined as

$$K_{\text{short}} \equiv \frac{m_1 m_2}{m_{12}^2} \sqrt{\frac{m_{123}}{m_{12}}} \left(\frac{a_{\text{in}}}{a_{\text{out}}} \right)^{7/2} V_{0,0} \sin I_{\text{obs}} = \frac{m_1 m_2}{m_{12}^2} \left(\frac{m_{123}}{m_{12}} \right)^{-2/3} \left(\frac{P_{\text{in}}}{P_{\text{out}}} \right)^{7/3} V_{0,0} \sin I_{\text{obs}}, \quad (4)$$

where $m_{12} \equiv m_1 + m_2$, $m_{123} \equiv m_{12} + m_*$,

$$V_{0,0} \equiv \frac{m_{12}}{m_{123}} a_{\text{out}} \nu_{\text{out}} = \left(\frac{2\pi \mathcal{G} m_{12}^3}{m_{123}^2 P_{\text{out}}} \right)^{1/3}, \quad (5)$$

with \mathcal{G} being Newton’s gravitational constant, and a_{in} , a_{out} , P_{in} , P_{out} and I_{obs} are the semi-major axes, orbital periods of inner and outer orbits, and the observed inclination, respectively. Equations (1), (4) and (5) can be derived from equations (21), (25)–(28) in [Morais & Correia \(2008\)](#), while they use somewhat a different notation.

Since we assume a triple with an inner binary companion throughout the present analysis, the orbital parameters with the subscript “out” are interpreted to be those estimated for the star-BH *binary* (with the subscript “obs” in Table 1 for Gaia BH1 and Gaia BH2). Similarly, we assume that $m_{12} = m_1 + m_2$ is equal to m_c in Table 1.

Figure 2 plots the contours of K_{short} in the $q_{21} \equiv m_2/m_1 - P_{\text{in}}$ plane; for Gaia BH1 (left) and Gaia BH2 (right). The shaded regions indicate those corresponding to dynamical instability condition for coplanar triples by [Mardling & Aarseth \(1999\)](#); [Aarseth & Mardling \(2001\)](#) (hereafter, MA01):

$$\frac{r_{\text{p,out}}}{a_{\text{in}}} > 2.8 \left(1 - 0.3 \frac{i_{\text{mut}}}{180^\circ} \right) \left[\left(1 + \frac{m_*}{m_{12}} \right) \frac{(1 + e_{\text{out}})}{\sqrt{1 - e_{\text{out}}}} \right]^{2/5}. \quad (6)$$

The condition (6) turned out to be a good approximation for coplanar triples ($i_{\text{mut}} = 0^\circ$). [Hayashi et al. \(2022, 2023\)](#) examined the *Lagrange* stability timescales of triples in general, and found that the condition (6) needs to be improved especially for inclined triples that exhibit the ZKL oscillations.

Figure 2 indicates that the expected values of K_{short} (dotted contours) are fairly small; at most $\mathcal{O}(10)$ m/s for Gaia BH1, and $\mathcal{O}(1)$ m/s for Gaia BH2. In reality, however, the observed semi-amplitude should be sensitive to the mutual phases of the three bodies, in particular for eccentric outer orbits as in the cases of both Gaia BH1 and Gaia BH2. While K_{short} in equation (4) is derived for circular orbits, we find that the effect of the outer eccentricity can be empirically taken into account by replacing a_{out} by $a_{\text{out}}(1 - e_{\text{out}})$ in equation (4), *i.e.*, $K_{\text{short}}(1 - e_{\text{obs}})^{-7/2}$ as plotted in red solid contours in Figure 2 (see Figure 3 for detail).

In the next subsection, we perform three-body simulations and show that the phase-dependent RV modulation amplitudes become even larger for Gaia BH1 and BH2 around the pericenter passages, due to their relatively large e_{obs} .

2.2. Numerical results

In order to predict the short-term RV modulations for Gaia BH1 and Gaia BH2 more quantitatively, we perform three-body simulations using [TSUNAMI](#) (see [Trani & Spera 2023](#)). The details of the procedure are described in [Hayashi et al. \(2020\)](#); [Hayashi & Suto \(2020\)](#); [Hayashi et al. \(2022, 2023\)](#).

Figure 3 shows results of the simulation for the inner equal-mass binaries ($m_1 = m_2 = m_c/2$). We fix the mean anomalies of $M_{\text{in}} = 30^\circ$, $M_{\text{out}} = 45^\circ$, pericenter arguments of $\omega_{\text{in}} = 0^\circ$, and $\omega_{\text{out}} = \omega_{\text{obs}}$

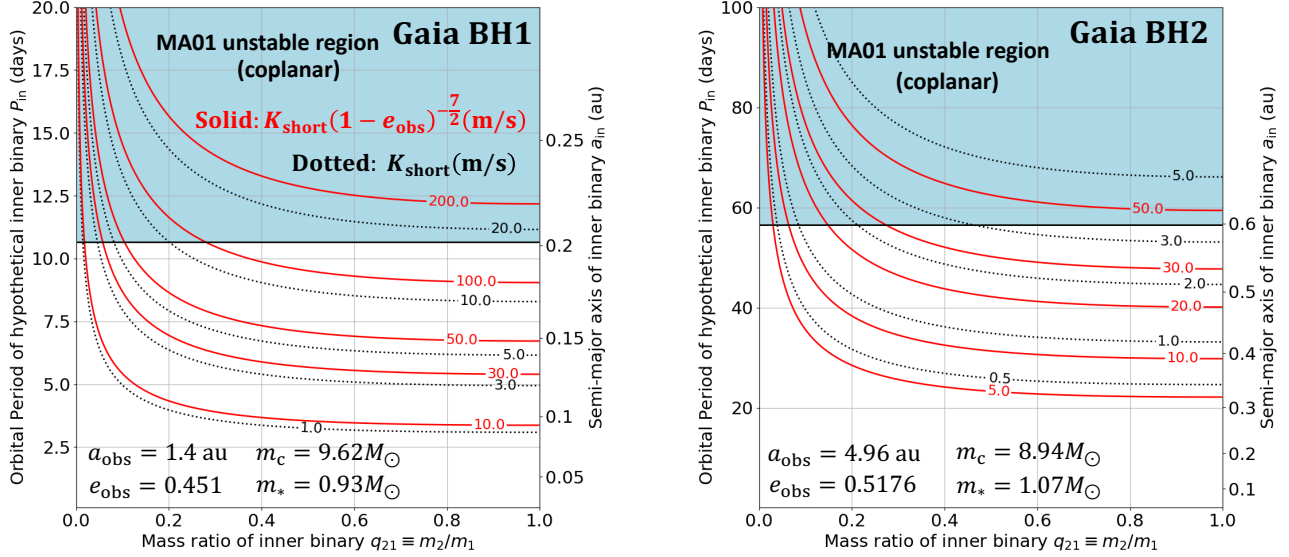


Figure 2. Contours of the characteristic semi-amplitude K_{short} (black dotted), equation (4) in the $q_{21} \equiv m_2/m_1 - P_{\text{in}}$ plane for Gaia BH1 (left) and Gaia BH2 (right). We assume coplanar triples ($i_{\text{mut}} = 0$). The shaded region indicates dynamically unstable triples according to equation (6). More accurate empirical predictions near the pericenter passage, $K_{\text{short}}(1 - e_{\text{obs}})^{-7/2}$, are plotted in red solid lines.

at the initial epoch. Then, the initial true anomalies f_j ($j = \text{in, out}$) in the simulations are computed from the mean anomalies M_j using the standard relations among the true anomaly f , eccentric anomaly E , mean anomaly M , and orbital eccentricity e :

$$\tan \frac{f_j}{2} = \sqrt{\frac{1 + e_j}{1 - e_j}} \tan \frac{E_j}{2} \quad (7)$$

and

$$M_j = E_j - e_j \sin E_j. \quad (8)$$

where variables with subscript j denote their values evaluated at the initial epoch.

In order to remove possible transient behavior due to the choice of initial phase angles, we first evolve the system over 100 outer orbital periods $P_{\text{out}} (= P_{\text{obs}})$. The top panels of Figure 3 is the resulting RV curve for $t = 100 P_{\text{obs}}$ to $101 P_{\text{obs}}$. Then, we fit the simulated RV data with the public code, `RadVel` (see [Fulton et al. 2018](#)) so as to remove the overall Kepler motion of the tertiary star. The resulting residuals (middle and bottom panels) represent the short-term RV modulations. We perform the `RadVel` fitting only for a single outer orbital period. If we do so over longer periods, the residuals become significantly larger in most of the periods because a long-term trend due to the three-body effect cannot be removed as long as purely two-body dynamics is assumed (e.g. [Hayashi & Suto 2020](#)). In other words, the short-term modulations in the middle and bottom panels of Figure 3 are the robust residuals reflecting $P_{\text{in}}/2$.

Left and right panels of Figure 3 correspond to Gaia BH1 with $P_{\text{in}} = 10$ days, and Gaia BH2 with $P_{\text{in}} = 50$ days, both of which are close to the dynamical stability limit (Figure 2). Red and blue curves show the results for the initial inner eccentricities of $e_{\text{in}} = 0$ and $e_{\text{in}} = 0.2$, respectively. The

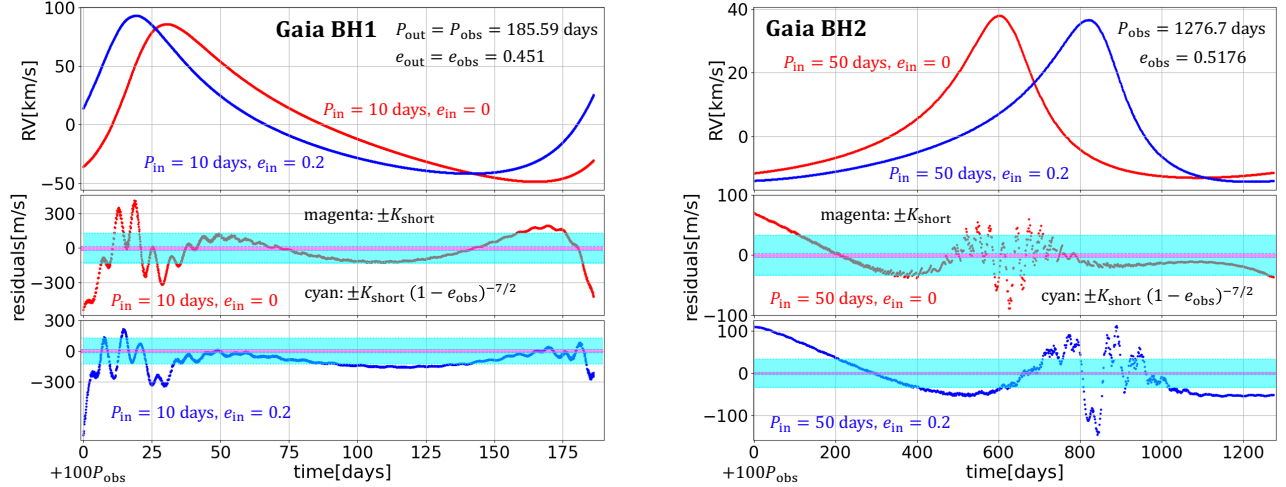


Figure 3. Examples of simulated radial velocity curves, and the residuals after removing the best-fit Kepler motion. The fittings are performed with `RadVel` (Fulton et al. 2018). We assume an equal-mass inner binary ($m_1 = m_2 = m_c/2$) for both systems. The left and right plots assume Gaia BH1 with $P_{\text{in}} = 10$ days, and Gaia BH2 with $P_{\text{in}} = 50$ days. The top panels shows the total RV curve with $e_{\text{in}} = 0$ (red) and $e_{\text{in}} = 0.2$ (blue), and the middle and bottom panels plot the corresponding RV residuals, respectively.

difference of e_{in} produces a small phase shift of the total and residual RV, but does not affect their amplitudes in practice.

For reference, we plot the analytic short-term modulation semi-amplitude $\pm K_{\text{short}}$, equation (4), and also $\pm K_{\text{short}}(1 - e_{\text{obs}})^{-7/2}$; see magenta and cyan regions in middle and bottom panels of Figure 3. Clearly, K_{short} significantly underestimates the simulated amplitudes. Indeed, the simulated RV modulations become even larger around the pericenter passage of the tertiary; the short-term RV modulations for Gaia BH1 and Gaia BH2 amount to ~ 300 m/s and ~ 100 m/s around the epoch. Those values are about 10–100 times larger than the analytic approximation K_{short} , equation (4), and may be detectable for Gaia BH1 from the observed RV residuals according to Figure 4 of El-Badry et al. (2023a).

2.3. Possible degeneracy between an S-type planet and an inner binary black hole companion

An S-type planet (i.e., a planet around the stellar member of the binary) would induce short-term RV modulations that are similar to those produced by an inner BBH as we presented in the above. The possible degeneracy of the short-term RV modulations between an inner binary companion in a triple system and a planet orbiting a star in a binary system has been pointed by Schneider & Cabrera (2006), and discussed by Morais & Correia (2008). Although precise spectroscopic measurements can break the degeneracy of the short-term RV signals between an inner binary and a planet (Morais & Correia 2008) in principle, Hayashi et al. (2020) argue that the degeneracy is difficult to be broken under realistic observational noises and limited cadences. Therefore, it is interesting to consider the correspondence of the two interpretations, especially for the future Gaia BH1 signals.

According to Hayashi et al. (2020), the RV semi-amplitude K_s induced by an S-type planet of mass M_{pl} in a circular and coplanar orbit is

$$K_s = \left(\frac{2\pi\mathcal{G}M_{\text{pl}}^3}{(m_* + M_{\text{pl}})^2 P_s} \right)^{1/3} \sin I_{\text{obs}} \approx \left(\frac{2\pi\mathcal{G}M_{\text{pl}}^3}{m_*^2 P_s} \right)^{1/3} \sin I_{\text{obs}}, \quad (9)$$

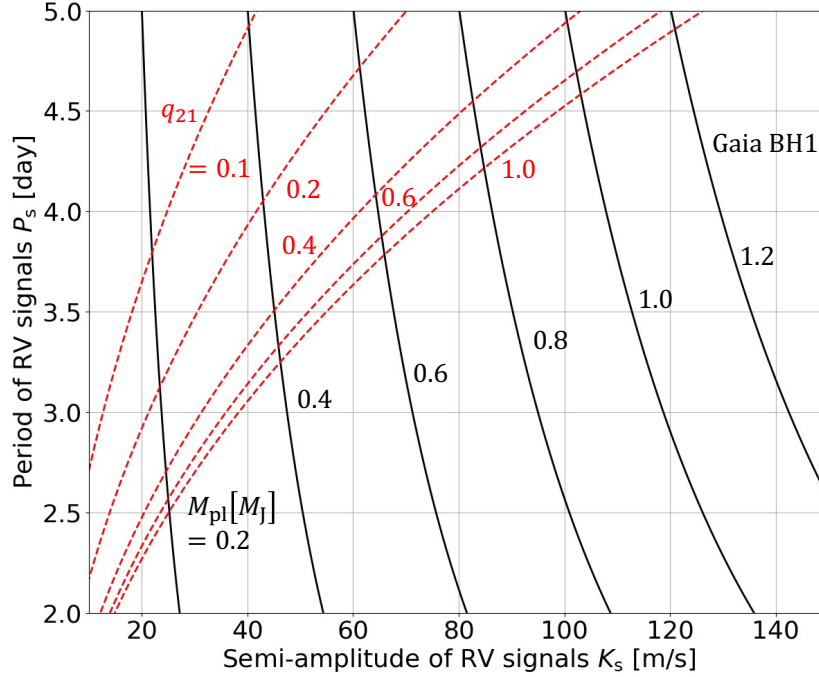


Figure 4. Mass ratio of inner BBH q_{21} (dashed) and the corresponding planet mass M_{pl} (solid) in RV signal semi-amplitude K_s –period P_s plane for Gaia BH1. We note that K_s and P_s are interpreted as RV semi-amplitude and period induced by a planet for the planet interpretation, while they are interpreted as $K_s = K_{\text{short}}(1 - e_{\text{obs}})^{-7/2}$ and $P_s = P_{\text{in}}/2$ for the BBH interpretation.

where P_s is the orbital period of planet. Figure 4 shows contours of M_{pl} (solid lines) and the mass ratio q_{21} (dashed lines) for the planet and BBH induced RV modulations of the semi-amplitude K_s and period P_s , respectively. For the planet interpretation, we assume a planet with a circular and coplanar orbit, while we assume $K_s = K_{\text{short}}(1 - e_{\text{obs}})^{-7/2}$ and $P_s = P_{\text{in}}/2$ for the BBH interpretation. Figure 4 clearly indicates that a close-in hot jupiter induces a short-term RV modulation similar to that we expect from an inner BBH. While it is a possible false-positive for the inner BBH search, it may reveal a first-ever planetary system orbiting a BH. Given the observed frequency of the close-in planet, it is likely to find such a system in future even if Gaia BH1 is not the one.

3. LONG-TERM RV MODULATIONS FOR MODERATELY INCLINED SYSTEMS: NODAL PRECESSION

Consider next non-coplanar triples, *i.e.*, the inner and outer orbits are mutually inclined. Hayashi & Suto (2020) pointed out that the long-term RV modulations of the tertiary body due to the nodal precession and the ZKL oscillations may carry interesting signatures of the hidden inner binary. The details of the inclined three-body dynamics are described in previous literature (e.g. Morais & Correia 2012; Naoz 2016).

In this section, we focus on the nodal precession in moderately inclined systems ($i_{\text{mut}} \lesssim 50^\circ$). First, we consider analytic approximations for the timescale and the RV modulation amplitude of the nodal precession. Then, we perform three-body simulations to present more quantitative prediction, and discuss the observational feasibility.

3.1. Analytic estimates

3.1.1. Nodal precession timescale

If e_{in} is initially small and i_{mut} is moderate ($i_{\text{mut}} \lesssim 50^\circ$), the outer ascending node Ω_{out} regularly precess with the following timescale P_Ω (e.g., Hayashi & Suto 2020):

$$P_\Omega = \frac{2\pi}{\dot{\Omega}_{\text{out}}} = \frac{\pi G_{\text{in}} G_{\text{out}}}{6 C_{\text{quad}} G_{\text{tot}} \cos i_{\text{mut}}}, \quad (10)$$

where C_{quad} is the quadrupole strength coefficient:

$$C_{\text{quad}} \equiv \frac{\mathcal{G}}{16} \frac{m_1 m_2}{m_{12}} \frac{m_*}{(1 - e_{\text{out}}^2)^{3/2}} \left(\frac{a_{\text{in}}^2}{a_{\text{out}}^3} \right), \quad (11)$$

and G_{in} , G_{out} , and G_{tot} are the amplitudes of inner, outer, and total angular momenta:

$$G_{\text{in}} = \mu_{\text{in}} \nu_{\text{in}} a_{\text{in}}^2 \sqrt{1 - e_{\text{in}}^2}, \quad (12)$$

$$G_{\text{out}} = \mu_{\text{out}} \nu_{\text{out}} a_{\text{out}}^2 \sqrt{1 - e_{\text{out}}^2}, \quad (13)$$

$$G_{\text{tot}} = \sqrt{G_{\text{in}}^2 + G_{\text{out}}^2 + 2G_{\text{in}}G_{\text{out}} \cos i_{\text{mut}}}. \quad (14)$$

In equations (12) and (13), μ_{in} and μ_{out} denote the reduced masses:

$$\mu_{\text{in}} \equiv \frac{m_1 m_2}{m_{12}} = \frac{q_{21} m_{12}}{(1 + q_{21})^2}, \quad (15)$$

$$\mu_{\text{out}} \equiv \frac{m_{12} m_*}{m_{123}}, \quad (16)$$

where $q_{21} \equiv m_2/m_1$ is the mass ratio of the inner binary.

It is convenient to introduce the ratio of the amplitudes of inner to outer angular momenta:

$$\xi \equiv \frac{G_{\text{in}}}{G_{\text{out}}} = \frac{q_{21}}{(1 + q_{21})^2} \sqrt{\frac{1 - e_{\text{in}}^2}{1 - e_{\text{out}}^2}} \left(\frac{m_{12}}{m_*} \right) \left(\frac{m_{123} P_{\text{in}}}{m_{12} P_{\text{out}}} \right)^{1/3}, \quad (17)$$

which is a key parameter that characterizes the long-term modulation due to the nodal precession.

Figure 5 plots ξ against P_{in} for Gaia BH1 and Gaia BH2 in solid and dashed lines; different colors correspond to $(q_{21}, e_{\text{in}}) = (1, 0)$, $(1, 0.3)$, $(0.1, 0)$, and $(0.1, 0.3)$. As equation (17) indicates, ξ is sensitive to q_{21} , but not to e_{in} as long as $e_{\text{in}}^2 \ll 1$. The realistic range of ξ values is shown in this figure for a given set of q_{21} and P_{in} . Due to dynamical stability, ξ cannot exceed about 1.2 and 0.9 for Gaia BH1 and Gaia BH2, respectively.

By rewriting equation (10) in terms of ξ as

$$P_\Omega = \frac{\pi}{6} \frac{\xi G_{\text{out}}}{C_{\text{quad}} \cos i_{\text{mut}}} \frac{1}{\sqrt{1 + 2\xi \cos i_{\text{mut}} + \xi^2}}, \quad (18)$$

equation (18) reduces to

$$\frac{P_\Omega}{P_{\text{out}}} = \frac{4q_{21}^3}{3(1 + q_{21})^6} \left(\frac{m_{12}^2 m_{123}^2}{m_*^4} \right) \frac{(1 - e_{\text{in}}^2)^2}{\xi^3 \cos i_{\text{mut}}} \frac{1}{\sqrt{1 + 2\xi \cos i_{\text{mut}} + \xi^2}}. \quad (19)$$

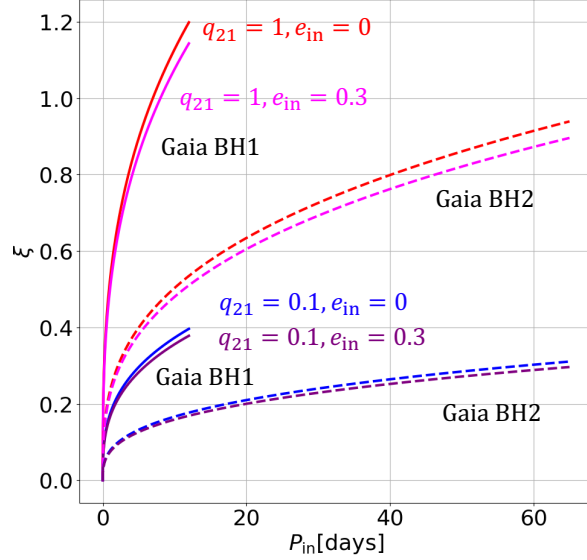


Figure 5. The ratio of the inner and outer angular momenta, ξ , plotted against P_{in} for different $q_{21} \equiv m_2/m_1$ and e_{in} . The solid and dashed lines correspond to Gaia BH1 and Gaia BH2, respectively.

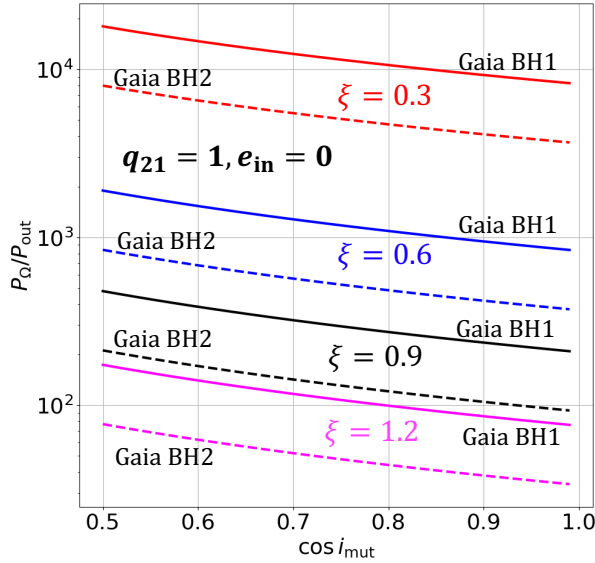


Figure 6. The normalized timescale of the nodal precession, $P_{\Omega}/P_{\text{out}}$, plotted against $\cos i_{\text{mut}}$ for different ξ . The solid and dashed lines correspond to Gaia BH1 and Gaia BH2, respectively. We fix $q_{21} = 1$ and $e_{\text{in}} = 0$ for simplicity.

Equation (19) implies that the nodal precession timescale is very sensitive to ξ . Figure 6 plots $P_{\Omega}/P_{\text{out}}$ as a function of $\cos i_{\text{mut}}$ for Gaia BH1 (solid) and BH2 (dashed) with $e_{\text{in}} = 0$ and $q_{21} = 1.0$. The plot also shows that $P_{\Omega}/P_{\text{out}}$ is not sensitive to i_{mut} as long as moderately inclined triples are considered.

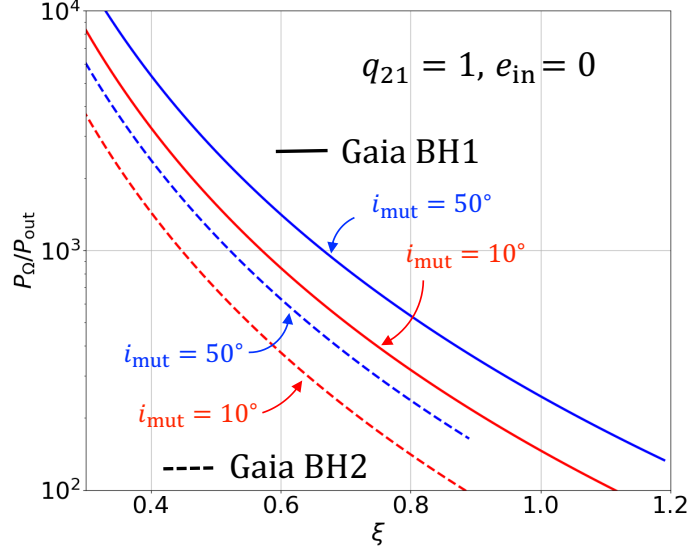


Figure 7. The normalized timescale of the nodal precession, P_Ω/P_{out} , plotted against ξ for $i_{\text{mut}} = 10^\circ$ (red) and 50° (blue). The solid and dashed curves correspond to Gaia BH1 and Gaia BH2, respectively. The q_{21} and e_{in} are fixed as 1.0 and 0.0, respectively.

Figure 7 shows P_Ω/P_{out} as a function of ξ for Gaia BH1 (solid) and BH2 (dashed) with $q_{21} = 1$ and $e_{\text{in}} = 0$. Since P_Ω is a strongly decreasing function of ξ , triples with a larger value of ξ are preferable for a successful detection of long-term RV modulations.

3.1.2. Relation between inclination angles

The long-term RV modulations due to the nodal precession are computed as a function of inclination angles illustrated in Figure 1. First, we derive a relation between i_{out} and i_{mut} , which proves to be useful in the later discussion.

The inner and outer inclinations i_{in} and i_{out} simply satisfy

$$i_{\text{in}} + i_{\text{out}} = i_{\text{mut}} \quad (20)$$

and

$$\sin i_{\text{out}} = \xi \sin i_{\text{in}}. \quad (21)$$

If we further neglect the ZKL oscillations and simply consider the nodal precession alone, i_{mut} is nearly constant. Therefore, the value of i_{out} is determined from equations (20) and (21), and also stays constant in practice.

For moderately inclined triples of $i_{\text{mut}} \lesssim 50^\circ$, we obtain

$$\sin i_{\text{out}} = \frac{\xi \sin i_{\text{mut}}}{\sqrt{1 + 2\xi \cos i_{\text{mut}} + \xi^2}}, \quad (22)$$

$$\cos i_{\text{out}} = \frac{1 + \xi \cos i_{\text{mut}}}{\sqrt{1 + 2\xi \cos i_{\text{mut}} + \xi^2}}. \quad (23)$$

Figure 8 plots the outer inclination i_{out} against i_{mut} for various values of ξ . The plot indicates that i_{out} becomes asymptotically close to i_{mut} as ξ increases. We intend to show Figure 8 as a generic

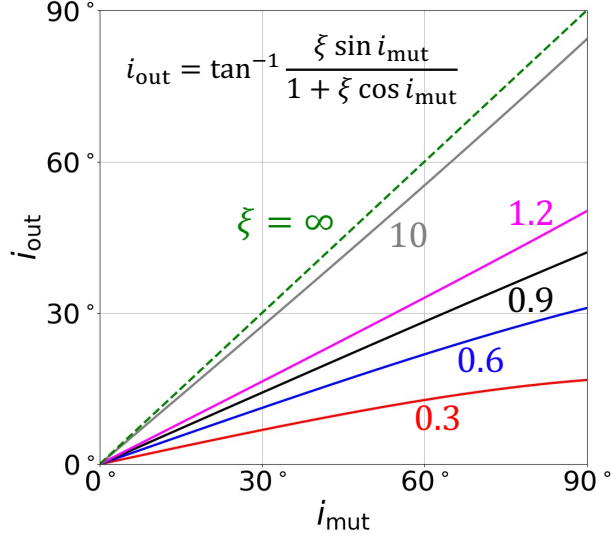


Figure 8. Relation of i_{out} and i_{mut} , equation (25) for different $\xi = 0.3, 0.6, 0.9, 1.2$ and 10 . For reference, we plot the dashed line that corresponds to the asymptotic limit of $\xi \rightarrow \infty$. Figures 2 and 5 imply that $\xi = 1.2$ and 0.9 roughly correspond to the maximum possible values for Gaia BH1 and Gaia BH2, respectively.

relation between two angles. In the cases of Gaia BH1 and Gaia BH2, however, large values of ξ are nonphysical due to dynamical stability requirements; $\xi \lesssim 1.2$ and $\xi \lesssim 0.9$ for Gaia BH1 and Gaia BH2, respectively. Thus, rather small values of i_{out} are allowed.

For moderately inclined triples in which the nodal precession (*i.e.* Ω_{out} precession) dominates the dynamics, Ω_{out} and $\phi(t)$ (see Figure 1) change gradually from 0° to 360° with timescale P_Ω . Thus, $I_{\text{obs}}(t)$ varies within the following range:

$$|I_{\text{los}} - i_{\text{out}}| < I_{\text{obs}}(t) < \min\{I_{\text{los}} + i_{\text{out}}, 360^\circ - (I_{\text{los}} + i_{\text{out}})\}. \quad (24)$$

We can insert in equation (24) the expression for i_{out} in terms of $i_{\text{mut}} (< 90^\circ)$ using the relation:

$$i_{\text{out}} = \tan^{-1} \frac{\xi \sin i_{\text{mut}}}{1 + \xi \cos i_{\text{mut}}}, \quad (25)$$

derived from equations (22) and (23).

Figure 9 shows the constraints on the inclination angles of Gaia BH1 (left) and Gaia BH2 (right) from the observed value of I_{obs} . If future observations detect any change of the RV semi-amplitude, or equivalently that of I_{obs} , this plot is useful in inferring the geometric configuration of the corresponding triple system.

The observed RV semi-amplitude $K(t)$ is proportional to $\sin I_{\text{obs}}(t)$. In the case of the nodal precession alone, we obtain from Figure 1

$$\cos I_{\text{obs}}(t) = \sin I_{\text{los}} \sin i_{\text{out}} \cos \phi(t) + \cos I_{\text{los}} \cos i_{\text{out}}. \quad (26)$$

Thus,

$$\sin I_{\text{obs}}(t) = \sqrt{1 - \sin^2 I_{\text{los}} \sin^2 i_{\text{out}} (\cos \phi(t) + \Gamma)^2}, \quad (27)$$

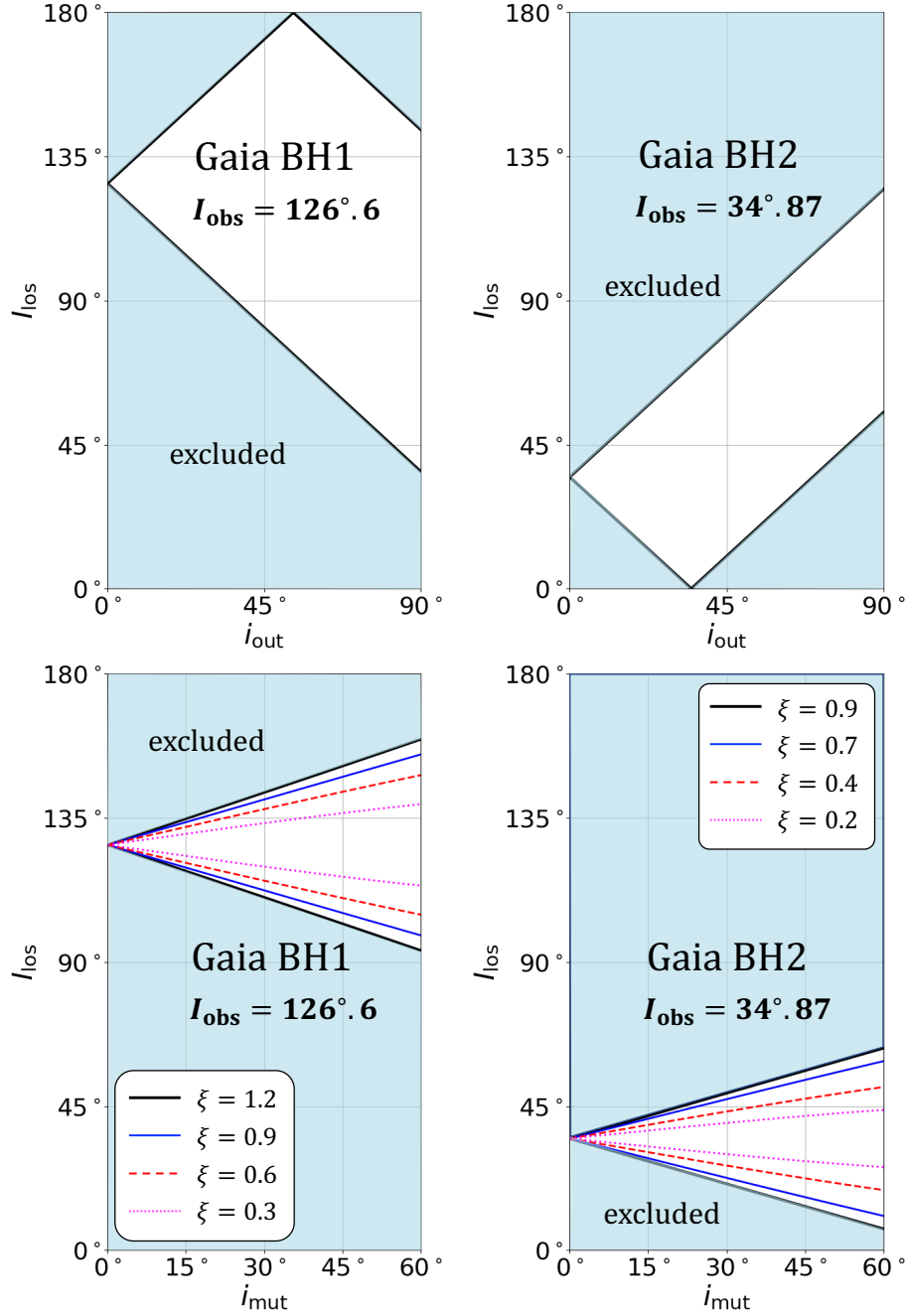


Figure 9. Relations between i_{out} and I_{los} (top), and i_{mut} and I_{los} (bottom). The left and right panels correspond to Gaia BH1 and Gaia BH2, respectively. Shaded regions in the top panels are excluded due to the observed value of the inclination I_{obs} (see Table 1). The bottom panels plot I_{los} against i_{mut} for given values of ξ . The region between two lines is permitted for each ξ , and the shaded regions correspond to $\xi > 1.2$ for Gaia BH1 and $\xi > 0.9$ for Gaia BH2, which are excluded from dynamical stability viewpoint.

where $\Gamma \equiv \cot i_{\text{out}} \cot I_{\text{los}}$, and the precession angle $\phi(t)$ varies from 0° to 360° periodically with the timescale of P_Ω as Ω_{out} precesses.

If $-1 \leq \Gamma \leq 1$, equation (27) becomes maximum (unity) when $\cos \phi = -\Gamma$. If $\Gamma < -1$ and $\Gamma > 1$, it becomes maximum when $\cos \phi = +1$ and -1 , respectively. Similarly, equation (27) becomes minimum when $\cos \phi = -1$ and $+1$, for $\Gamma < 0$ and $\Gamma > 0$, respectively. It is amusing to note that the periodic change of the above RV semi-amplitude is basically identical to photometric variations for an oblique rotating star with surface inhomogeneities (Suto et al. 2022, 2023).

The above argument is simply summarized as

$$K_{\max}/V_0 = \begin{cases} 1 & (-1 \leq \Gamma \leq 1) \\ |\sin(I_{\text{los}} - i_{\text{out}})| & (\Gamma < -1) \\ |\sin(I_{\text{los}} + i_{\text{out}})| & (1 < \Gamma) \end{cases} \quad (28)$$

and

$$K_{\min}/V_0 = \begin{cases} |\sin(I_{\text{los}} + i_{\text{out}})| & (\Gamma < 0) \\ |\sin(I_{\text{los}} - i_{\text{out}})| & (0 < \Gamma) \end{cases}, \quad (29)$$

where V_0 is the RV semi-amplitude for an edge-on system:

$$V_0 \equiv \frac{V_{0,0}}{\sqrt{1 - e_{\text{out}}^2}} = \frac{1}{\sqrt{1 - e_{\text{out}}^2}} \left(\frac{2\pi \mathcal{G} m_{12}^3}{m_{123}^2 P_{\text{out}}} \right)^{1/3}. \quad (30)$$

If future long-term RV monitoring (over the duration exceeding P_Ω) identifies the RV modulation of Gaia BH1 and BH2, equations (28) and (29) determine the inclination angles of the line-of-sight and the outer orbits, I_{los} and i_{out} , separately. If the dark companion is a single BH, instead of BBH, $i_{\text{out}} = 0^\circ$ and $I_{\text{los}} = I_{\text{obs}}$ always (see Figure 1). The inner binarity of the dark companion may be revealed by $i_{\text{out}} \neq 0^\circ$. Note that there is a parameter degeneracy of $I_{\text{obs}} \leftrightarrow 180^\circ - I_{\text{obs}}$ in the RV observation, but the astrometry indeed breaks this degeneracy.

Figure 10 summarizes the expected fractional change of the RV semi-amplitude, Δ_K , in the $P_{\text{in}} - P_\Omega$ plane for Gaia BH1 (left) and Gaia BH2 (right). Specifically, we define Δ_K using equations (28) and (29):

$$\Delta_K \equiv \frac{K_{\max} - K_{\min}}{V_0}. \quad (31)$$

For simplicity, we here assume $e_{\text{in}} = 0$ and $q_{21} = 1$ for both Gaia BH1 and Gaia BH2. In addition, we fix $I_{\text{los}} = 120^\circ$ and 30° for Gaia BH1 and Gaia BH2, respectively, corresponding to the values close to their I_{obs} ; see Table 1.

The light-blue regions correspond to the dynamically unstable region from MA01 (see equation (6)). We note that for high mutual inclination ($i_{\text{mut}} \gtrsim 50^\circ$), the analytic discussion based on the nodal precession becomes invalid since the ZKL oscillations become important. For moderate inclination, however, we can safely estimate Δ_K , and corresponding P_{in} and P_Ω . Figure 10 implies that $\Delta_K = 0.2$ – 0.4 variations are expected within 100 yrs for Gaia BH1 if $P_{\text{in}} = 5$ – 10 days, while unrealistically long observational duration is required to detect the similar level of variations for Gaia BH2.

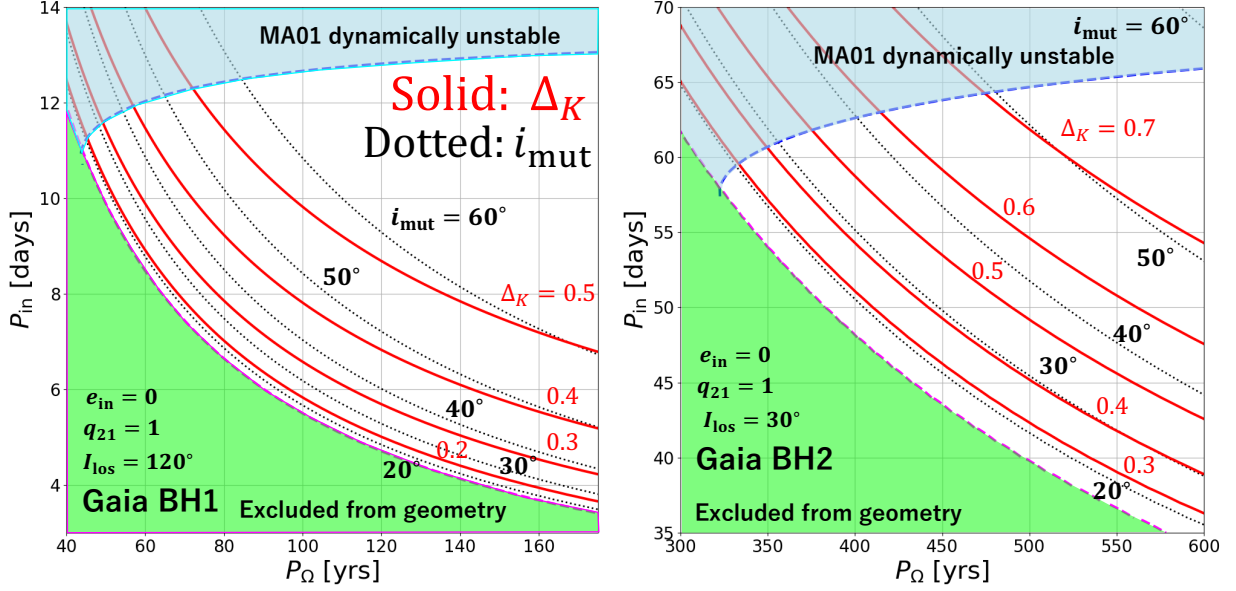


Figure 10. Contours of the RV semi-amplitude changes Δ_K (red-solid) and the mutual inclination i_{mut} (black-dotted) from nodal precession on $P_\Omega - P_{\text{in}}$ plane for Gaia BH1 (left) and Gaia BH2 (right). The light-blue regions correspond to the dynamically unstable region from MA01. The green regions are excluded from the observed value of I_{obs} ; see equation (24). For relatively large mutual inclination, $i_{\text{mut}} \gtrsim 50^\circ$, the predictions of these plots become less reliable because the ZKL oscillations become important.

3.2. Numerical results

In order to discuss the observational feasibility, we perform three-body numerical simulations with TSUNAMI, and present examples of the expected long-term RV modulations. We fix the initial phases ($M_{\text{in}} = 30^\circ$, $M_{\text{out}} = 45^\circ$, $\omega_{\text{in}} = 0^\circ$, $\omega_{\text{out}} = \omega_{\text{obs}}$), and assume $m_1 = m_2$, $P_{\text{in}} = 10$ days (Gaia BH1) and $P_{\text{in}} = 50$ days (Gaia BH2), $e_{\text{in}} = 0$. We additionally assume $I_{\text{los}} = 120^\circ$ (Gaia BH1) and $I_{\text{los}} = 30^\circ$ (Gaia BH2), and $i_{\text{mut}} = 20^\circ$.

The top panels of Figure 11 show the simulated RV semi-amplitudes against t/P_Ω for Gaia BH1 (left) and Gaia BH2 (right), respectively. The red and blue curves indicate the envelope of the radial velocity $K(t)/V_0$, *i.e.*, neglecting the periodic changes over P_{out} , which we define as $\text{RV}_{\text{max}}/V_0$ and $\text{RV}_{\text{min}}/V_0$. The normalized RV semi-amplitude $K/V_0 \equiv (\text{RV}_{\text{max}} - \text{RV}_{\text{min}})/2V_0$ is plotted in solid black curves, which should be compared with an analytic prediction, equation (31) with equations (28) and (29). In the plots, we show the analytically estimated Δ_K as magenta regions, and the expected semi-amplitude change from equation (27) as dotted green curves. We chose the initial phases $\phi(t=0)$ so that they agree with the values from the simulations.

As expected, the ZKL oscillations are negligible for the present case ($i_{\text{mut}} = 20^\circ$ initially), and the mutual inclination is nearly constant over the period of P_Ω . The simulated RV semi-amplitude changes almost sinusoidally with a period of $\sim P_\Omega$ (black curve), and its fractional change Δ_K is indeed in good agreement with the value predicted from the analytic approximation; $\Delta_K \approx 0.2$ for Gaia BH1, and $\Delta_K \approx 0.3$ for Gaia BH2, see Figure 10.

The example for Gaia BH1 indicates the RV semi-amplitude change of as large as 17 km/s, corresponding to $\Delta_K = 0.2$, within $P_\Omega/2 \approx 26$ yrs, depending on the phase. Furthermore, the zero-point of the RV curve also changes significantly. Thus, future long-term RV monitoring of Gaia BH1 should

provide strong constraints on, or even detect, its inner BBH. On the contrary, the case of Gaia BH2 is very difficult because its P_Ω is too long.

4. LONG-TERM RV MODULATIONS FOR SIGNIFICANTLY INCLINED SYSTEMS: ZKL OSCILLATIONS

Finally, we consider triple systems whose inner binary orbit is significantly inclined, $i_{\text{mut}} > 50^\circ$, relative to the outer orbit. In this case, analytic discussion is not easy due to the strong ZKL oscillations. Thus, we present examples of numerical simulations alone.

The middle and bottom panels of Figure 11 are the same as the top panels except that their initial mutual inclinations are $i_{\text{mut}} = 60^\circ$ and $i_{\text{mut}} = 90^\circ$, respectively. Note that they are plotted against t/P_{out} , and their long-term modulation period is roughly consistent with the quadrupole ZKL timescale (e.g. Antognini 2015):

$$\frac{T_{\text{ZKL}}}{P_{\text{out}}} = \frac{m_{123}P_{\text{out}}}{m_3P_{\text{in}}}(1 - e_{\text{out}}^2)^{3/2} \approx 130 \left(\frac{m_{123}}{10M_\odot} \right) \left(\frac{m_3}{1M_\odot} \right)^{-1} \left(\frac{P_{\text{out}}/P_{\text{in}}}{20} \right) \left[1 - \left(\frac{e_{\text{out}}}{0.5} \right)^2 \right]^{3/2}. \quad (32)$$

The middle panels, with $i_{\text{mut}} = 60^\circ$ initially, indicate that the amplitude of the ZKL oscillations are still modest in this example, and the resulting semi-amplitude change (black curves) is roughly sinusoidal as expected for nodal precession alone. Moreover, the analytic prediction of Δ_K , equation (31), agrees with the simulated value within ten percent.

In contrast, the bottom plots, with $i_{\text{mut}} = 90^\circ$ initially, show non-trivial RV curves, due to the strong ZKL oscillations. For most of the time, the systems stay at mutually orthogonal orbits, but suddenly move to $i_{\text{mut}} \approx 40^\circ$. While the change of the mutual inclination is very periodic roughly with the ZKL timescale T_{ZKL} , equation (32), the corresponding RV semi-amplitude changes are no longer periodic. Therefore, long-term RV monitoring of such systems may detect the significant change of the RV semi-amplitude even for relatively short timescales, or barely no change for long duration, depending on the phase of the observation over the sporadic behavior represented in the bottom panels of Figure 11.

5. SUMMARY AND DISCUSSION

Triple systems are ubiquitous in the universe, and trigger a wide variety of interesting observable events in astronomy. While nearly a hundred of BBHs have been discovered from the GWs emitted at the final instance of their coalescence, there is no candidate for triples including two BHs yet. Needless to say, such triples are fascinating targets for observational astronomy. Furthermore, star-BBH or even triple BH systems may provide an important mechanism to accelerate the GW merger of the detected BBHs (e.g. Liu & Lai 2018; Trani et al. 2022).

Formation and evolution of stellar triples are fundamental, but theoretically challenging, problems in broad areas of astrophysics. Their proper understanding requires many complicated physical processes, including the evolution of common envelope phases, supernova explosions, and the subsequent dynamics of the resulting compact objects (e.g. Toonen et al. 2021). Thus, future discoveries of star-BH binaries and star-BBH triples that we consider in the present paper would shed complementary observational insights that are useful in constructing and testing theoretical models.

Hayashi et al. (2020) and Hayashi & Suto (2020) have proposed a methodology to discover a hidden inner BBH in star-BH binary candidates from the radial velocity modulations of the orbiting

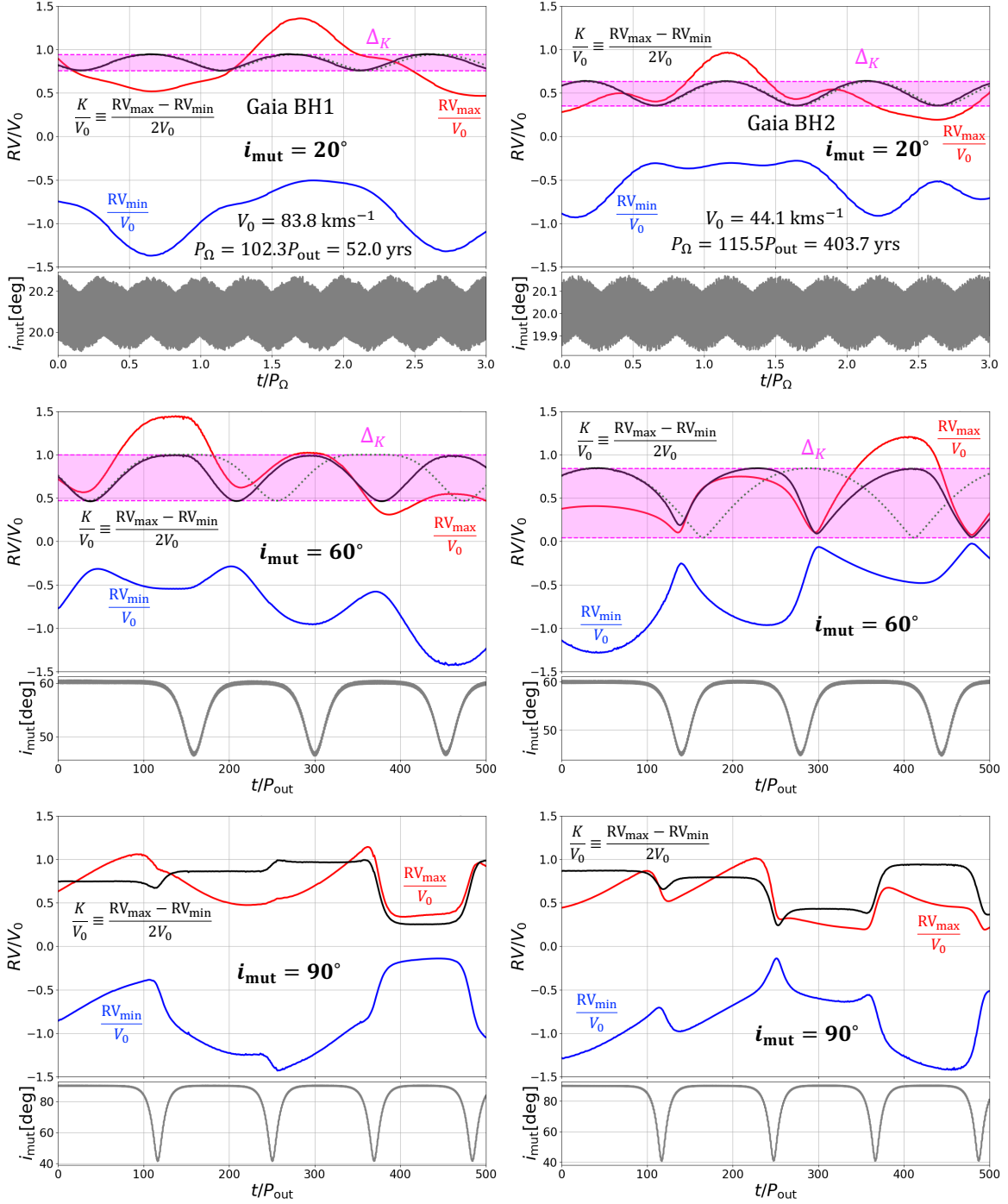


Figure 11. Example of evolution of simulated RV semi-amplitudes and the mutual inclination angles for the initial values of $i_{\text{mut}} = 20^\circ$ (top), 60° (middle), and 90° (bottom). The left and right panels correspond to Gaia BH1 ($P_{\text{in}} = 10$ days and $I_{\text{los}} = 120^\circ$) and Gaia BH2 ($P_{\text{in}} = 50$ days and $I_{\text{los}} = 30^\circ$), respectively. For simplicity, we assume the equal-mass inner binary ($q_{12} = 1$) in an initially circular orbit ($e_{\text{in}} = 0$). For reference, the range of the analytic estimate of Δ_K , equation (31), is plotted in magenta regions, and the expected semi-amplitude change, from equation (27), is plotted as dotted green curves. Equation (10) diverges for $i_{\text{mut}} = 90^\circ$, and we do not show the analytic predictions in those cases.

(tertiary) star. Recent discoveries of such systems, Gaia BH1 and BH2 (El-Badry et al. 2023a,b; Chakrabarti et al. 2023; Tanikawa et al. 2023), provide a great opportunity to examine the feasibility of their methodology in detail as a *proof of concept*. Even if the dark companion of Gaia BH1 and BH2 turn out to be a single BH instead of a BBH, the analysis presented here is readily applicable for future star-BH candidates that remain to be discovered. The results of our proof-of-concept study are summarized below.

- (1) **short-term RV modulations induced by the inner BBH:** Inner BBH generates a small-amplitude modulation of period P_{in} on the RV of the tertiary star. The semi-amplitudes based on an analytic approximation are $\mathcal{O}(10)$ m/s for Gaia BH1, and $\mathcal{O}(1)$ m/s for Gaia BH2, if the tertiary is on a coplanar and circular orbit. In reality, relatively large eccentricities of $e_{\text{obs}} \sim 0.5$ for both systems are expected to significantly increase the semi-amplitude. Our numerical simulations indicate that the semi-amplitude of the short-term RV modulation increases by more than a factor of $(1 - e_{\text{out}})^{-7/2} (\approx 11)$ near the pericenter passage. Thus, the resulting amplitudes amount to ~ 300 m/s for Gaia BH1, and ~ 100 m/s for Gaia BH2 at their pericenter passage phases. We conclude that high-cadence and precise RV followups near the pericenter passages of the star are promising to search for possible inner BBHs for star-BH candidates with large e_{obs} .
- (2) **long-term RV modulations induced by the nodal precession:** If the orbit of the inner BBH is moderately inclined relative to that of the tertiary, $i_{\text{mut}} \lesssim 50^\circ$, the nodal precession generates long-term modulations of the radial velocity, or equivalently of the inclination I_{obs} of the tertiary relative to the observer’s line of sight. Unlike the short-term RV modulation, the nodal precession changes the RV semi-amplitude of the tertiary by a factor of $\sin I_{\text{obs}}$. Thus, the change of the RV semi-amplitude, $\Delta_K V_0$, is significantly larger than that of the short-term modulation, but its modulation period P_Ω may be unrealistically long. Our examples from three-body simulations (equal-mass circular BBH with $P_{\text{in}} = 10$ days) predict the RV semi-amplitude change of 17 km/s within ~ 26 yrs for Gaia BH1, assuming that the line-of-sight inclination $I_{\text{los}} = 120^\circ$ is close to the observed inclination $I_{\text{obs}} = 126^\circ.6$. For Gaia BH2, the nodal precession timescale is too long to be detectable within a reasonable observation duration. More importantly, we confirm that our simple analytic estimates of Δ_K and P_Ω reproduce well the simulation results.
- (3) **long-term RV modulation induced by the ZKL oscillations:** For highly inclined triples, the ZKL oscillations induce the drastic and non-periodic RV semi-amplitude change, and analytic approximation becomes less reliable than the case with the nodal precession alone. Thus, numerical simulations are required to make quantitative predictions. We confirm that the timescale of the corresponding RV modulations are consistent with the ZKL timescale T_{ZKL} , which is roughly $\sim 100P_{\text{out}}$ for our fiducial cases for Gaia BH1 ($P_{\text{out}} \sim 190$ days) and Gaia BH2 ($P_{\text{out}} \sim 1300$ days). Due to the rather sporadic and abrupt change of the RV semi-amplitude due to the ZKL oscillations, we may be able to detect the signatures of the long-term RV modulation depending on the observational phase.

We have demonstrated the feasibility of detecting an inner BBH from RV follow-ups of star-BH binary candidates, if some of them are indeed star-BBH triples. We studied the presently available

best targets, Gaia BH1 and Gaia BH2, as a proof-of-concept, but found that future monitoring of Gaia BH1 may indeed detect an inner BBH within a reasonable timescale. Current gravitational-wave data seem to point to a possible mass gap of BHs between $3 \sim 6M_{\odot}$, but its reality is still controversial. Thus, an inner BBH in Gaia BH1, if detected, has a huge impact on the formation scenarios of BHs in general.

The three observable signatures of the RV modulations of the tertiary discussed in the above summary are quite generic, and can be applied to more candidates from future Gaia data in a straightforward manner. We also mention that this method is applicable to tertiary pulsar - BBH triple systems using the pulsar timing analysis, instead of RV monitoring (Hayashi & Suto 2021). Furthermore, the long-term inclination modulation is sufficiently large to be identified from the orbital parameters determined by astrometry in ~ 10 years from now. For instance, Liu et al. (2022) propose that the secular eccentricity variations induced by the apsidal precession resonances are potentially detectable with Gaia astrometry observations.

At this point, it is quite uncertain if such star-BBH and even pulsar-BBH triples exist within our reachable horizon. Nevertheless, we would like to conclude by referring to a universal principle that “everything not forbidden is compulsory” (White 1939; Thorne & Zytzkow 1975; Sagan 1985).

ACKNOWLEDGMENTS

T.H. thanks Kareem El-Badry for fruitful discussion on the possible binary companion in Gaia BH1 during the workshop “The Renaissance of Stellar Black-Hole Detections in The Local Group”, held from June 26 to 30, 2023, at the Lorentz Center in Leiden University. T.H. gratefully acknowledges the fellowship by Japan Society for the Promotion of Science (JSPS). This work is supported partly by the JSPS KAKENHI grant Nos. JP19H01947 and JP23H01212 (Y.S.), JP21J11378 and JP23KJ1153 (T.H.), and JP21K13914 (A.A.T.).

REFERENCES

- Aarseth, S. J., & Mardling, R. A. 2001, *Astronomical Society of the Pacific Conference Series*, Vol. 229, *The Formation and Evolution of Multiple Star Systems*, ed. P. Podsiadlowski, S. Rappaport, A. R. King, F. D’Antona, & L. Burderi (Astronomical Society of the Pacific), 77
- Abbott, B. P., Abbott, R., Abbott, T. D., et al. 2016, *Physical Review Letters*, 116, 061102, doi: [10.1103/PhysRevLett.116.061102](https://doi.org/10.1103/PhysRevLett.116.061102)
- Antognini, J. M. O. 2015, *MNRAS*, 452, 3610, doi: [10.1093/mnras/stv1552](https://doi.org/10.1093/mnras/stv1552)
- Belczynski, K., Dominik, M., Repetto, S., Holz, D. E., & Fryer, C. L. 2012, *ArXiv e-prints*. <https://arxiv.org/abs/1208.0358>
- Belczynski, K., Holz, D. E., Bulik, T., & O’Shaughnessy, R. 2016a, *Nature*, 534, 512, doi: [10.1038/nature18322](https://doi.org/10.1038/nature18322)
- Belczynski, K., Kalogera, V., & Bulik, T. 2002, *ApJ*, 572, 407, doi: [10.1086/340304](https://doi.org/10.1086/340304)
- Belczynski, K., Repetto, S., Holz, D. E., et al. 2016b, *ApJ*, 819, 108, doi: [10.3847/0004-637X/819/2/108](https://doi.org/10.3847/0004-637X/819/2/108)
- Belczynski, K., Taam, R. E., Kalogera, V., Rasio, F. A., & Bulik, T. 2007, *ApJ*, 662, 504, doi: [10.1086/513562](https://doi.org/10.1086/513562)
- Bird, S., Cholis, I., Muñoz, J. B., et al. 2016, *Physical Review Letters*, 116, 201301, doi: [10.1103/PhysRevLett.116.201301](https://doi.org/10.1103/PhysRevLett.116.201301)
- Breivik, K., Chatterjee, S., & Larson, S. L. 2017, *ApJL*, 850, L13, doi: [10.3847/2041-8213/aa97d5](https://doi.org/10.3847/2041-8213/aa97d5)
- Chakrabarti, S., Simon, J. D., Craig, P. A., et al. 2023, *AJ*, 166, 6, doi: [10.3847/1538-3881/accf21](https://doi.org/10.3847/1538-3881/accf21)
- Chawla, C., Chatterjee, S., Breivik, K., et al. 2022, *ApJ*, 931, 107, doi: [10.3847/1538-4357/ac60a5](https://doi.org/10.3847/1538-4357/ac60a5)
- Dominik, M., Belczynski, K., Fryer, C., et al. 2012, *ApJ*, 759, 52, doi: [10.1088/0004-637X/759/1/52](https://doi.org/10.1088/0004-637X/759/1/52)

- . 2013, *ApJ*, 779, 72,
doi: [10.1088/0004-637X/779/1/72](https://doi.org/10.1088/0004-637X/779/1/72)
- El-Badry, K., Rix, H.-W., Quataert, E., et al. 2023a, *MNRAS*, 518, 1057,
doi: [10.1093/mnras/stac3140](https://doi.org/10.1093/mnras/stac3140)
- El-Badry, K., Rix, H.-W., Cendes, Y., et al. 2023b, *MNRAS*, 521, 4323,
doi: [10.1093/mnras/stad799](https://doi.org/10.1093/mnras/stad799)
- Fragione, G., Martinez, M. A. S., Kremer, K., et al. 2020, *ApJ*, 900, 16,
doi: [10.3847/1538-4357/aba89b](https://doi.org/10.3847/1538-4357/aba89b)
- Fulton, B. J., Petigura, E. A., Blunt, S., & Sinukoff, E. 2018, *PASP*, 130, 044504,
doi: [10.1088/1538-3873/aaaaa8](https://doi.org/10.1088/1538-3873/aaaaa8)
- Gaia Collaboration, Prusti, T., de Bruijne, J. H. J., et al. 2016, *A&A*, 595, A1,
doi: [10.1051/0004-6361/201629272](https://doi.org/10.1051/0004-6361/201629272)
- Gaia Collaboration, Arenou, F., Babusiaux, C., et al. 2022, arXiv e-prints, arXiv:2206.05595.
<https://arxiv.org/abs/2206.05595>
- Hayashi, T., & Suto, Y. 2020, *ApJ*, 897, 29,
doi: [10.3847/1538-4357/ab97ad](https://doi.org/10.3847/1538-4357/ab97ad)
- . 2021, *ApJ*, 907, 48,
doi: [10.3847/1538-4357/abcec6](https://doi.org/10.3847/1538-4357/abcec6)
- Hayashi, T., Trani, A. A., & Suto, Y. 2022, *ApJ*, 939, 81, doi: [10.3847/1538-4357/ac8f48](https://doi.org/10.3847/1538-4357/ac8f48)
- . 2023, *ApJ*, 943, 58,
doi: [10.3847/1538-4357/acac1e](https://doi.org/10.3847/1538-4357/acac1e)
- Hayashi, T., Wang, S., & Suto, Y. 2020, *The Astrophysical Journal*, 890, 112,
doi: [10.3847/1538-4357/ab6de6](https://doi.org/10.3847/1538-4357/ab6de6)
- Ioka, K., Tanaka, T., & Nakamura, T. 1999, *PhRvD*, 60, 083512,
doi: [10.1103/PhysRevD.60.083512](https://doi.org/10.1103/PhysRevD.60.083512)
- Kawanaka, N., Yamaguchi, M., Piran, T., & Bulik, T. 2016, *Proceedings of the International Astronomical Union*, 12, 41,
doi: [10.1017/S1743921316012606](https://doi.org/10.1017/S1743921316012606)
- Kinugawa, T., Inayoshi, K., Hotokezaka, K., Nakauchi, D., & Nakamura, T. 2014, *MNRAS*, 442, 2963, doi: [10.1093/mnras/stu1022](https://doi.org/10.1093/mnras/stu1022)
- Kinugawa, T., Miyamoto, A., Kanda, N., & Nakamura, T. 2016, *MNRAS*, 456, 1093,
doi: [10.1093/mnras/stv2624](https://doi.org/10.1093/mnras/stv2624)
- Kocsis, B., Suyama, T., Tanaka, T., & Yokoyama, S. 2018, *ApJ*, 854, 41,
doi: [10.3847/1538-4357/aaa7f4](https://doi.org/10.3847/1538-4357/aaa7f4)
- Kozai, Y. 1962, *AJ*, 67, 591, doi: [10.1086/108790](https://doi.org/10.1086/108790)
- Lidov, M. L. 1962, *Planet. Space Sci.*, 9, 719,
doi: [10.1016/0032-0633\(62\)90129-0](https://doi.org/10.1016/0032-0633(62)90129-0)
- Liu, B., D’Orazio, D. J., Vigna-Gómez, A., & Samsing, J. 2022, *PhRvD*, 106, 123010,
doi: [10.1103/PhysRevD.106.123010](https://doi.org/10.1103/PhysRevD.106.123010)
- Liu, B., & Lai, D. 2018, *ApJ*, 863, 68,
doi: [10.3847/1538-4357/aad09f](https://doi.org/10.3847/1538-4357/aad09f)
- Mardling, R., & Aarseth, S. 1999, in *NATO Advanced Science Institutes (ASI) Series C*, Vol. 522, *NATO Advanced Science Institutes (ASI) Series C*, ed. B. A. Steves & A. E. Roy (Springer), 385
- Mashian, N., & Loeb, A. 2017, *MNRAS*, 470, 2611, doi: [10.1093/mnras/stx1410](https://doi.org/10.1093/mnras/stx1410)
- Masuda, K., & Hotokezaka, K. 2019, *ApJ*, 883, 169, doi: [10.3847/1538-4357/ab3a4f](https://doi.org/10.3847/1538-4357/ab3a4f)
- Michaely, E., & Naoz, S. 2022, *ApJ*, 936, 184,
doi: [10.3847/1538-4357/ac8a92](https://doi.org/10.3847/1538-4357/ac8a92)
- Michaely, E., & Perets, H. B. 2016, *MNRAS*, 458, 4188, doi: [10.1093/mnras/stw368](https://doi.org/10.1093/mnras/stw368)
- . 2019, *ApJL*, 887, L36,
doi: [10.3847/2041-8213/ab5b9b](https://doi.org/10.3847/2041-8213/ab5b9b)
- Morais, M. H. M., & Correia, A. C. M. 2008, *A&A*, 491, 899,
doi: [10.1051/0004-6361:200810741](https://doi.org/10.1051/0004-6361:200810741)
- . 2012, *MNRAS*, 419, 3447,
doi: [10.1111/j.1365-2966.2011.19986.x](https://doi.org/10.1111/j.1365-2966.2011.19986.x)
- Naoz, S. 2016, *ARA&A*, 54, 441,
doi: [10.1146/annurev-astro-081915-023315](https://doi.org/10.1146/annurev-astro-081915-023315)
- O’Leary, R. M., Kocsis, B., & Loeb, A. 2009, *MNRAS*, 395, 2127,
doi: [10.1111/j.1365-2966.2009.14653.x](https://doi.org/10.1111/j.1365-2966.2009.14653.x)
- Portegies Zwart, S. F., & McMillan, S. L. W. 2000, *ApJL*, 528, L17, doi: [10.1086/312422](https://doi.org/10.1086/312422)
- Rastello, S., Iorio, G., Mapelli, M., et al. 2023, arXiv e-prints, arXiv:2306.14679,
doi: [10.48550/arXiv.2306.14679](https://doi.org/10.48550/arXiv.2306.14679)
- Ricker, G. R., Winn, J. N., Vanderspek, R., et al. 2014, in *Society of Photo-Optical Instrumentation Engineers (SPIE) Conference Series*, Vol. 9143, *Space Telescopes and Instrumentation 2014: Optical, Infrared, and Millimeter Wave*, ed. J. Oschmann, Jacobus M., M. Clampin, G. G. Fazio, & H. A. MacEwen, 914320, doi: [10.1117/12.2063489](https://doi.org/10.1117/12.2063489)
- Rodriguez, C. L., Haster, C.-J., Chatterjee, S., Kalogera, V., & Rasio, F. A. 2016, *ApJL*, 824, L8, doi: [10.3847/2041-8205/824/1/L8](https://doi.org/10.3847/2041-8205/824/1/L8)
- Sagan, C. 1985, *Contact* (New York: Simon and Schuster)

- Sasaki, M., Suyama, T., Tanaka, T., & Yokoyama, S. 2016, *Physical Review Letters*, 117, 061101, doi: [10.1103/PhysRevLett.117.061101](https://doi.org/10.1103/PhysRevLett.117.061101)
- . 2018, *Classical and Quantum Gravity*, 35, 063001, doi: [10.1088/1361-6382/aaa7b4](https://doi.org/10.1088/1361-6382/aaa7b4)
- Schneider, J., & Cabrera, J. 2006, *A&A*, 445, 1159, doi: [10.1051/0004-6361:20053447](https://doi.org/10.1051/0004-6361:20053447)
- Shikauchi, M., Kumamoto, J., Tanikawa, A., & Fujii, M. S. 2020, *PASJ*, doi: [10.1093/pasj/psaa030](https://doi.org/10.1093/pasj/psaa030)
- Spera, M., Mapelli, M., Giacobbo, N., et al. 2019, *MNRAS*, 485, 889, doi: [10.1093/mnras/stz359](https://doi.org/10.1093/mnras/stz359)
- Suto, Y., Sasaki, S., Aizawa, M., Fujisawa, K., & Kashiyama, K. 2023, *PASJ*, 75, 103, doi: [10.1093/pasj/psac093](https://doi.org/10.1093/pasj/psac093)
- Suto, Y., Sasaki, S., Nakagawa, Y., & Benomar, O. 2022, *PASJ*, 74, 857, doi: [10.1093/pasj/psac039](https://doi.org/10.1093/pasj/psac039)
- Tagawa, H., Umemura, M., & Gouda, N. 2016, *MNRAS*, 462, 3812, doi: [10.1093/mnras/stw1877](https://doi.org/10.1093/mnras/stw1877)
- Tanikawa, A., Hattori, K., Kawanaka, N., et al. 2023, *ApJ*, 946, 79, doi: [10.3847/1538-4357/acbf36](https://doi.org/10.3847/1538-4357/acbf36)
- The LIGO Scientific Collaboration, the Virgo Collaboration, the KAGRA Collaboration, et al. 2021, arXiv e-prints, arXiv:2111.03606. <https://arxiv.org/abs/2111.03606>
- Thorne, K. S., & Zytlow, A. N. 1975, *ApJL*, 199, L19, doi: [10.1086/181839](https://doi.org/10.1086/181839)
- Toonen, S., Boekholt, T. C. N., & Portegies Zwart, S. 2021, arXiv e-prints, arXiv:2108.04272. <https://arxiv.org/abs/2108.04272>
- Trani, A. A., Rastello, S., Di Carlo, U. N., et al. 2022, *MNRAS*, 511, 1362, doi: [10.1093/mnras/stac122](https://doi.org/10.1093/mnras/stac122)
- Trani, A. A., & Spera, M. 2023, *IAU Symposium*, 362, 404, doi: [10.1017/S1743921322001818](https://doi.org/10.1017/S1743921322001818)
- von Zeipel, H. 1910, *Astronomische Nachrichten*, 183, 345, doi: [10.1002/asna.19091832202](https://doi.org/10.1002/asna.19091832202)
- White, T. 1939, *The Once and Future King* (London: Collins)
- Yamaguchi, M. S., Kawanaka, N., Bulik, T., & Piran, T. 2018, *ApJ*, 861, 21, doi: [10.3847/1538-4357/aac5ec](https://doi.org/10.3847/1538-4357/aac5ec)